

## Defects in lamellar diblock copolymers: Chevron- and $\Omega$ -shaped tilt boundaries

Yoav Tsoori and David Andelman

*School of Physics and Astronomy, Raymond and Beverly Sackler Faculty of Exact Sciences, Tel Aviv University, 69978 Ramat Aviv, Israel*

M. Schick

*Department of Physics, Box 351560, University of Washington, Seattle, Washington 98195-1560*

(Received 24 May 1999; revised manuscript received 27 October 1999)

The lamellar phase in diblock copolymer systems appears as a result of a competition between molecular and entropic forces, which selects a preferred periodicity of the lamellae. Grain boundaries are formed when two grains of different orientations meet. We investigate the case where the lamellae meet symmetrically with respect to the interface. The form of the interface strongly depends on the angle,  $\theta$ , between the normals of the grains. When this angle is small, the lamellae transform smoothly from one orientation to the other, creating the chevron morphology. As  $\theta$  increases, a gradual transition is observed to an omega morphology characterized by a protrusion of the lamellae along the interface between the two phases. We present a theoretical approach to find these tilt boundaries in two-dimensional systems, based on a Ginzburg-Landau expansion of the free energy, which describes the appearance of lamellae. Close to the tips at which lamellae from different grains meet, these lamellae are distorted. To find this distortion for small angles, we use a phase variation ansatz in which one assumes that the wave vector of the bulk lamellar phase depends on the distance from the interface. Minimization of the free energy gives an expression for the order parameter  $\phi(x,y)$ . The results describe the chevron morphology very well. For larger angles, a different approach is used. We linearize  $\phi$  around its bulk value  $\phi_L$  and expand the free energy to second order in their difference. Minimization of the free energy results in a linear fourth-order differential equation for the distortion field, with proper constraints, similar to the Mathieu equation. The calculated monomer profile and line tension agree qualitatively with transmission electron microscope experiments, and with full numerical solution of the same problem.

PACS number(s): 61.25.Hq, 83.70.Hq, 61.41.+e, 02.30.Jr

### I. INTRODUCTION

The lamellar phase is one of the possible phases with spatial modulations that can be found in a wide variety of physical and chemical systems. These include diblock copolymer melts, mixtures of diblock and homopolymers, aqueous solutions of lipids or surfactants, Langmuir monolayers, and magnetic garnet films [1]. Modulated phases are the result of a competition between forces, one of which prefers ordering characterized by a nonzero wavenumber, while the other prefers a homogeneous (disordered) state. Below we shall employ the language appropriate to block-copolymers, but our work applies equally to other systems.

We consider diblock copolymer melts in which the two polymer blocks are incompatible. This incompatibility is characterized by a positive Flory parameter  $\chi$ . Because of the covalent chemical bond between the *A* and *B* blocks, the system cannot undergo a true macrophase separation. Instead it undergoes a *microphase separation* characterized by *A*- and *B*-rich domains of a finite size. Various modulated phases such as lamellar, hexagonal, and cubic are observed [2–7] depending upon the  $\chi$  parameter as well as on the relative lengths of *A* and *B* blocks. In most cases, the  $\chi$  parameter depends inversely on the temperature. Hence, the lamellar and other modulated phases will not be stable at high temperatures and the polymer melt will be in a disordered state.

The equilibrium behavior of diblock copolymers in the bulk is by now well understood [5–7]. Single domain bulk

phases, however, are rarely observed in experiments because it is extremely difficult to completely anneal defects. In most cases, due to very slow dynamics and energy barriers, the microstructural ordering is limited to finite-size domains (or grains) separated by grain boundaries. These defects are very common to block copolymer systems and are readily observed in experiments [3,4].

Because these domain boundaries and defects are so abundant in polymer melts, it is of interest to study their energetics and other characteristics. In this paper, we concentrate on the relatively simple situation of domain boundaries in lamellar phases in which there is no twist between the two grains, only a tilt, as is shown schematically in Fig. 1(a). The system is translationally invariant along the *z* direction and can be described by its *x-y* cross section only, reducing it to an effective two-dimensional system. As can be seen in Fig. 1(a), the distance between lamellae along the grain boundary  $d_x$  is larger than the lamellae spacing in bulk  $d$ , by a factor of  $1/\cos(\theta/2)$ . This causes an increase in the local free energy density related to the grain boundary.

The experiments of Gido and Thomas [3] and Hashimoto and coworkers [4] show that the response of the system to this increase in free energy depends strongly on the tilt angle  $\theta$  between the grains. The so-called *chevron* morphology [3] occurs when the angle is small. In such a situation, lamellae transform smoothly from one orientation to the other, creating *V*-shaped tips. The rounding of these tips reduces the interfacial area between lamellae at the expense of introducing a curvature energy. For block copolymers the profile

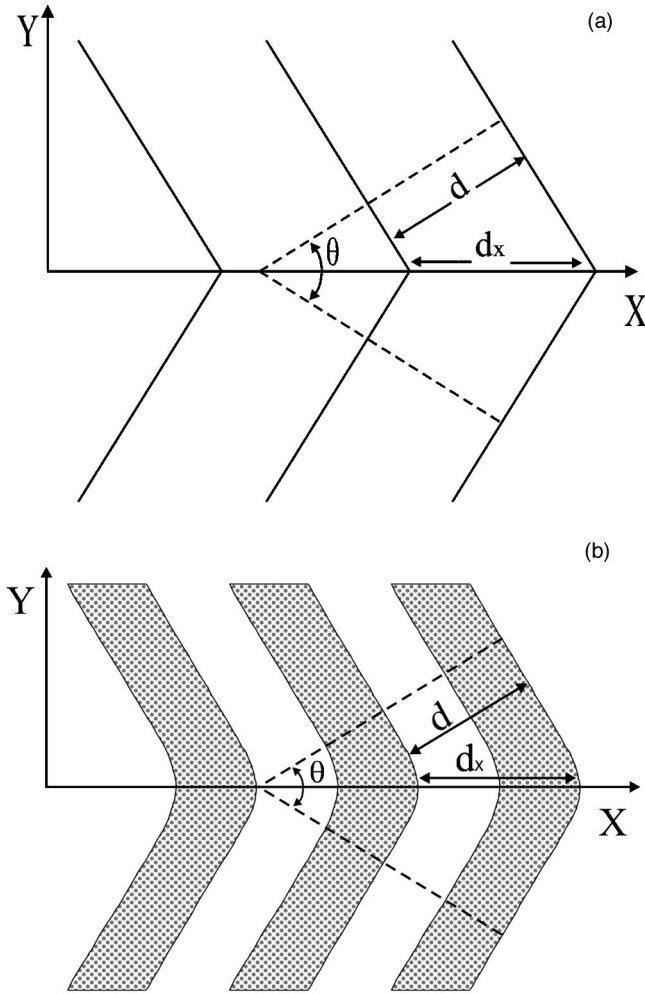


FIG. 1. A schematic drawing of the geometry of the system. In (a) the tilt angle  $\theta$  between the normal of the two lamellar phases is shown. The bulk periodicity  $d$  is smaller than the local periodicity  $d_x = d/\cos(\theta/2)$  at the interface,  $y=0$ . In (b) a schematic drawing of a chevron morphology with rounded V-shaped tips is shown.

shape at the tip is determined by the local relaxation of the stretched chains. The chevron morphology is shown (schematically) in Fig. 1(b) and again in Fig. 2(a). A gradual transition to an *omega-shaped* tip is observed when  $\theta$  is increased, as seen in Fig. 2(b). This morphology is characterized by protrusions of the lamellae along the interface between the two phases. The protrusions can be understood as a different attempt of the system to reduce the cost of the boundary, while still complying with the geometrical constraints. Essentially, the system tries to create a lamella similar to those in the bulk but that is aligned along the interface itself.

The basic phenomenology of these grain boundaries was presented by Gido and Thomas [3]. Netz, Andelman, and Schick [2] then considered the phenomenon employing a Ginzburg-Landau free energy, which was minimized numerically, and obtained both the chevron and omega morphologies. Matsen [8] considered the block-copolymer system explicitly and employed self-consistent field theory. Not only did this produce the chevron and omega morphologies for small and intermediate angles, respectively, but also a symmetry-broken omega for large enough angles. In the lat-

ter case, the response (and shape) of lamellae composed of one of the blocks differs from that of the other. Such symmetry-broken boundaries were indeed observed by Gido and Thomas [3].

In Sec. II, we adopt the Ginzburg-Landau free energy functional employed earlier [2]. The advantages to using this functional are its simplicity and generality, while retaining the essential ingredients that capture the behavior of the system. In contrast to the complete minimization of the free energy functional, which requires a numerical calculation, we shall employ here a simple ansatz for the form of the grain boundary in order to obtain analytic results. Recently, similar methods were employed to obtain analytically the interface between the lamellar and disordered phases of diblock copolymers [9]. Our motivation is to demonstrate that the essence of these interesting morphologies does not depend on strong segregation conditions or a large number of Fourier components, and so should be observable in all systems with modulated phases.

The chevron structure is obtained by using the bulk lamellar phase solution with a constant amplitude, but with varying wave vector. Minimizing the free energy subject to the proper geometrical constraints, we find an equation for the wave vector. This is done in Sec. III. Beyond the chevron regime (i.e., for large interdomain angles), this approach will not be adequate, because the amplitude of modulations will have to vary as well. To this end, we expand  $\phi(x,y)$  around the two bulk lamellar phases, giving rise to an equation for a small distortion field. Close to the interface, the sharp tips of the lamellar phase [see Fig. 1(a)] are smoothed out and the protrusion characteristic of the omega morphology appears. Far away from the interface, the disturbance vanishes and the bulk lamellar phase is recovered, as is shown in Sec. IV. In Sec. IV A, we discuss some features of our method, the analogy to, and the differences from the Schrödinger equation for electrons in a one-dimensional periodic potential (known also as the Mathieu equation). In Sec. V, we report our results, and discuss them in Sec. VI.

## II. MODEL

An order parameter  $\psi(\mathbf{R}) = [\psi_A(\mathbf{R}) - \psi_B(\mathbf{R})]$  is defined as the difference in local  $A$  and  $B$  monomer volume fractions. We employ the following Ginzburg-Landau free energy functional of this order parameter

$$\frac{\mathcal{F}[\psi]}{k_B T} = \int \left[ \frac{c_1}{2} \psi^2 + \frac{c_2}{12} \psi^4 + \frac{c_3}{2} (\nabla \psi)^2 + \frac{c_4}{2} (\nabla^2 \psi)^2 \right] d^3 \mathbf{R}, \quad (1)$$

where  $k_B$  is the Boltzmann constant, and  $T$  is the temperature. With  $c_1$  and  $c_2$  positive, the first two terms favor a uniform, disordered state. The coefficient of the third term,  $c_3$ , is negative and therefore induces the system to a modulated, ordered phase. The Laplacian squared term ensures that these modulations are not too large. This type of free energy functional (and some variants of it) has been successfully used to describe the bulk phase of diblock copolymers [5,6], amphiphilic systems [10], Langmuir films [11], and magnetic (garnet) films [12].

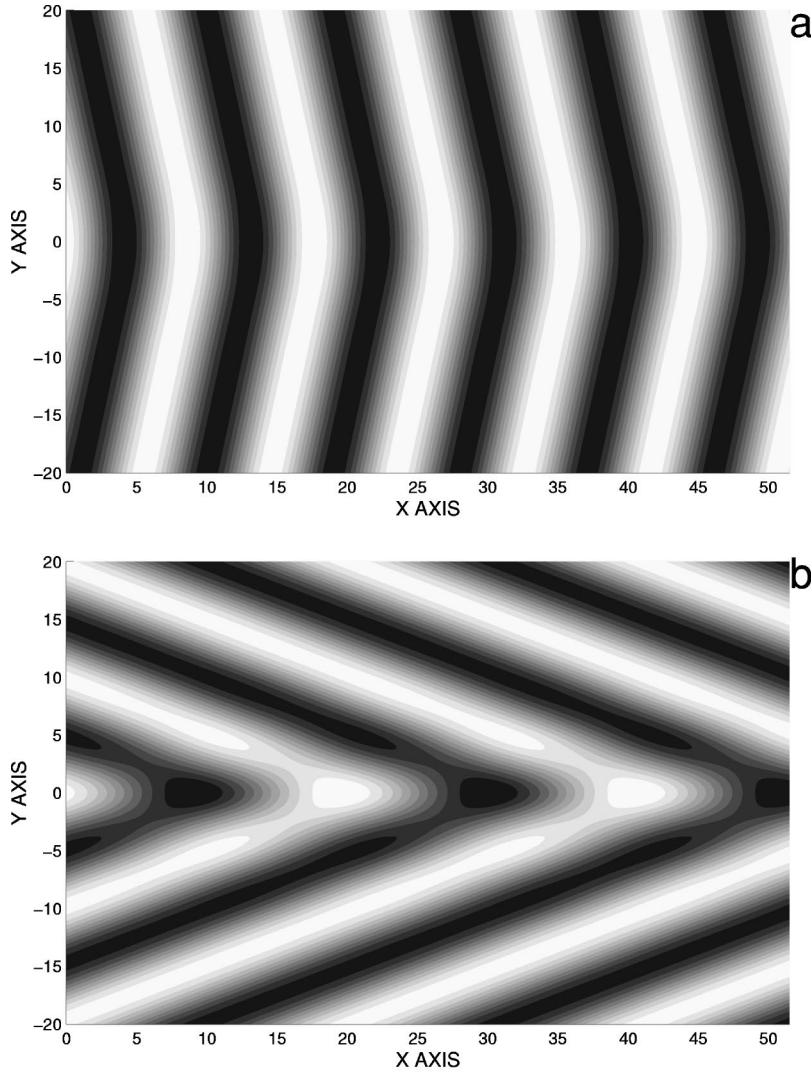


FIG. 2. Black and white contour plot of the order parameter profile  $\phi_\Omega$ , as obtained from the profile solutions of Sec. IV. The grayness denotes the value of the order parameter ( $A/B$  relative volume fraction). Black domains are  $A$  rich, white domains are  $B$ -rich. The value of the interaction parameter is  $\chi=1$  and the average difference of monomer volume fractions is  $\phi_0=0$ . For the small angle ( $\theta=20^\circ$ , top plot) chevron morphology appears, while for  $\theta=130^\circ$  (bottom plot) omega takes over.

Assuming an infinite system that is nonuniform only along one direction, one can minimize this free energy to obtain a solution describing the lamellar phase  $\psi_L \propto \cos(\mathbf{Q} \cdot \mathbf{R})$ . One readily finds that the transition to the lamellar phase first occurs at a wave number  $Q = (-c_3/2c_4)^{1/2}$ . It is convenient, therefore, to introduce the dimensionless position vector  $\mathbf{r}$  via

$$\mathbf{r} \equiv \left( \frac{-c_3}{c_4} \right)^{1/2} \mathbf{R} \quad (2)$$

and further to rescale the order parameter

$$\phi(\mathbf{r}) \equiv \left( \frac{c_2 c_4}{c_3} \right)^{1/2} \psi(\mathbf{R}) \quad (3)$$

and the free energy

$$F[\phi] \equiv \left( \frac{-c_2^2 c_4}{c_3^5} \right)^{1/2} \frac{\mathcal{F}[\psi]}{k_B T} \quad (4)$$

so that the dimensionless and rescaled free energy functional takes the form

$$F[\phi] = \int \left[ \frac{c_1 c_4}{2c_3^2} \phi^2 + \frac{1}{12} \phi^4 - \frac{1}{2} (\nabla \phi)^2 + \frac{1}{2} (\nabla^2 \phi)^2 \right] d^3 \mathbf{r}. \quad (5)$$

The coefficient  $c_1$  changes sign as the interaction strength increases or temperature decreases. In a polymer system,  $c_1$  can be shown to be proportional to  $1 - \chi_f/\chi_f^*$ , where  $\chi_f$  is the Flory parameter [13], and  $\chi_f^*$  the value of this parameter at which the coefficient  $c_1$  passes through zero [14].

To make contact with Ref. [2], we set the ratio of coefficients  $c_1 c_4 / c_3^2$  to be equal to  $1 - \chi$ . For this particular choice of coefficients, the free energy functional becomes

$$F[\phi] = \int \left[ \frac{1}{2} (1 - \chi) \phi^2 + \frac{1}{12} \phi^4 - \frac{1}{2} (\nabla \phi)^2 + \frac{1}{2} (\nabla^2 \phi)^2 \right] d^3 \mathbf{r} \quad (6)$$

The bulk lamellar phase, with wave vector in the  $x$  direction, is described by

$$\phi_L = \phi_0 + \phi_q \cos(qx) \quad (7)$$

with  $\phi_0$  the average volume fraction difference,  $q \equiv Q(-c_3/c_4)^{-1/2} = 1/\sqrt{2}$  the optimal wave vector, and  $\phi_q = 2\sqrt{\chi - \phi_0^2 - 3/4}$  the amplitude of the variations [9]. It

can be shown [5–7] that this lamellar phase is the thermodynamical stable phase in a range of the system parameters:  $\phi_0$  and  $\chi$ . For block copolymers,  $\phi_0$  is proportional to the difference in the average volume fractions of  $A$  and  $B$  monomers.

Upon substitution of  $\phi_L$  into Eq. (6), one obtains the free energy per unit volume of the bulk lamellar phase

$$\frac{F[\phi_L]}{V} = \frac{1}{2} \left[ (1-\chi)\phi_0^2 + \frac{\phi_0^4}{6} \right] - \frac{1}{2} \left[ \chi - \frac{3}{4} - \phi_0^2 \right]^2, \quad (8)$$

where  $V = \int d^3 \mathbf{r}$  is the rescaled, dimensionless, volume of the system.

Some remarks are now in order. First, as was mentioned in the introduction, the free energy (6) can have other non-lamellar modulated solutions [2,15]. We will not consider them in this paper since our aim is to study defects inside *lamellar* phases. Second, the validity of a single-optimal mode can be justified in the weak segregation limit (i.e., near a critical point or a weak first-order transition). Far from the critical point, higher harmonics are needed to describe the optimal lamellar phase [2,8]. In addition, very close to the critical point corrections due to fluctuations are important [16,17].

We now turn to the tilt-boundary problem, where two lamellar domains, both lying parallel to the  $x$ - $y$  plane, meet with an angle  $\theta$  between their normals [see Fig. 1(a)]. The  $x$  axis is along the line interface between the two lamellar domains. The  $y$  axis is perpendicular to it. In these variables the lamellae in the two grains are described by

$$\phi_L = \phi_0 + \phi_q \cos(q_x x \mp q_y y), \quad (9)$$

where  $q_x \equiv q \cos(\theta/2)$  and  $q_y \equiv q \sin(\theta/2)$  are the components of the optimal wave vector,  $\mathbf{q} = (q_x, q_y)$ . Their inverses provide characteristic length scales in the  $x$  and  $y$  directions, respectively. The  $y < 0$  half plane is a reflection through the  $x$  axis of the  $y > 0$  half plane, so it is sufficient to consider only the upper half plane,  $y > 0$ . The system is periodic along the  $x$  axis, with wavelength  $d_x = 2\pi/q_x = 2\pi/[q \cos(\theta/2)]$ .

### III. DESCRIPTION OF THE CHEVRON MORPHOLOGY

For small tilt angles, the lamellae transform smoothly from one orientation to the other, showing the chevron morphology. We will assume that for small enough tilt angles, the only change of the functional form of the order parameter is through the wave vector [18,19]. The aim of this section is to show that, in the chevron regime, the behavior of the system close to the interface is, in essence, quite similar to that far from the interface. The diagonal lines in Fig. 1(a) show each bulk lamellar phase in its respective half plane, and the sharp tips which result from their intersection. These sharp tips will be smoothed out in the chevron morphology, Fig. 1(b).

We use the following ansatz for the order parameter

$$\phi_c(\mathbf{r}) = \phi_0 + \phi_q \cos[q_x x + q_y u(y)], \quad (10)$$

where the amplitude  $\phi_q$  is identical to that in the bulk solution  $\phi_L$ . This choice is motivated by the fact that, in the chevron morphology, the amplitude of the order parameter

appear to be rather constant, while it is the phase which changes smoothly from one grain to the other. The local direction and magnitude of the wave vector depends on the distance  $y$  from the  $x$  axis. Far away from the interface, the lamellae must return to their bulk orientation, implying

$$\lim_{y \rightarrow \pm\infty} u(y) = \mp (q_y/q_x)y = \mp \tan(\theta/2)y \quad (11)$$

and at the interface, the continuous function  $u(y)$  satisfies

$$\lim_{y \rightarrow 0} u(y) = 0. \quad (12)$$

Symmetry with respect to inversion across the  $x$  axis means that

$$\left. \frac{\partial \phi_c}{\partial y} \right|_{y=0} = -\phi_q q_x u'(0) \sin(q_x x) = 0, \quad (13)$$

which implies

$$u'(0) = 0. \quad (14)$$

We insert the form (10) into the free energy functional (6). The integration over  $x$  and  $z$  can be carried out. The remaining integration over  $y$  shows that  $F[\phi_c]$  is proportional to the dimensionless, rescaled, volume  $V$  of the system. This reflects the fact that the order parameter profile approaches its bulk value far from the grain boundary. Subtraction of the bulk free energy produces a functional for the free energy per unit area of the grain boundary. After simple manipulation, one finds the expression

$$\begin{aligned} \gamma &\equiv \frac{F[\phi_c] - F[\phi_L]}{A} \\ &= \frac{\phi_q^2}{4} \sin^2(\theta/2) \\ &\quad \times \int_0^\infty dy \left[ \left( \frac{ds}{dy} \right)^2 + \frac{\sin^2(\theta/2)}{2} (1-s^2)^2 \right], \end{aligned} \quad (15)$$

where

$$s(y) \equiv -\frac{1}{\tan(\theta/2)} \frac{du}{dy}. \quad (16)$$

From the boundary condition, Eq. (11), one sees that far from the grain boundary  $s$  attains the value  $\pm 1$  and that its derivative vanishes. It is clear, therefore, that if  $s$  approaches its limiting value sufficiently quickly, the grain boundary free energy is finite. This is indeed the case.

The Euler-Lagrange equation, which minimizes the grain boundary free energy is

$$\frac{d^2 s}{dy^2} + s(1-s^2)\sin^2(\theta/2) = 0, \quad (17)$$

which has the solution

$$s = \pm \tanh \left[ \frac{1}{\sqrt{2}} \sin(\theta/2)y \right] = \pm \tanh q_y y \quad (18)$$

and

$$u(y) = \mp \frac{1}{q_y} \tan(\theta/2) \ln \cosh(q_y y). \quad (19)$$

We have thus found the order parameter profile following the initial ansatz (10)

$$\phi_c(x, y) = \phi_0 + \phi_q \cos\{q_x x - \ln[2 \cosh(q_y y)]\}. \quad (20)$$

The grain boundary free energy can now be obtained by inserting the profile solution, Eq. (20), into Eq. (15)

$$\gamma = \frac{2}{3} \phi_q^2 q_y^3 \sim \sin^3(\theta/2). \quad (21)$$

The order parameter we have calculated describes the chevrons very well. The tips of the  $V$ -shape structure are rounded off, and far away from the interface the bulk phase is restored. The values of the grain-boundary energy are close to those obtained from full numerical minimization of the free energy functional (6), see Ref. [2]. The expression (21) for the grain boundary energy shows a  $\theta^3$  scaling for small angles [18].

The width of the grain boundary is the characteristic distance over which the phase of the order parameter profile deviates from its bulk value. From the profile of Eq. (20), we see that this distance is  $1/q_y$ , which, for small grain boundary angles, varies as  $1/\theta$ , in accord with well-established results [18].

The deficiency of the above approach is that it does not give the cross over from the chevron to the omega morphology. For this end, another approach will be used in the next section.

#### IV. DESCRIBING THE $\Omega$ MORPHOLOGY

As the tilt angle  $\theta$  is increased, the chevron structure is deformed more and more. For large angles the lamellae protrude along the interface between the grains, creating the  $\Omega$ -shaped structure. In this regime, the polymer profile is qualitatively altered, and calls for a different approach.

In this section, we use the bulk-phase solution as a zeroth-order approximation and determine a correction to it; that is we write

$$\phi(x, y) = \phi_L(x, y) + \delta\phi(x, y). \quad (22)$$

Of course our ansatz for the chevrons, which was motivated by the smooth variation of phase, which they display, can also be written in this form with a particular choice of  $\delta\phi$ . Below, we shall choose a different  $\delta\phi$  based on the observation that the distortion of the omegas is well localized near the grain boundary.

After substitution of this form into Eq. (6) the free energy can be written as a sum of two parts

$$F[\phi] = F_L + \gamma A, \quad (23)$$

where  $F_L = F[\phi_L]$  is the bulk free energy, proportional to the volume and  $\gamma A$  is the grain boundary energy proportional to the area of the boundary. To second order in  $\delta\phi$ , the latter is

$$\begin{aligned} \gamma[\delta\phi] = & \frac{1}{A} \int \left\{ \left[ (1-\chi)\phi_L + \frac{1}{3}\phi_L^3 \right] \delta\phi + \frac{1}{2}(1-\chi + \phi_L^2) \delta\phi^2 \right. \\ & + \nabla^2 \phi_L \nabla^2 \delta\phi + \frac{1}{2} (\nabla^2 \delta\phi)^2 - \nabla \phi_L \nabla \delta\phi \\ & \left. - \frac{1}{2} (\nabla \delta\phi)^2 \right\} d^3 \mathbf{r}. \end{aligned} \quad (24)$$

Since  $\phi_L$  minimizes  $F_L$ , we need to find the function  $\delta\phi(x, y)$  that minimizes  $\gamma$ . This, in principle, is done via the Euler-Lagrange equation.

The boundary conditions for  $\phi(x, y)$  follows from the symmetry of the grain boundaries, and from the requirement that  $\phi$  approach its bulk value away from the interface:

$$\left. \frac{\partial^n \phi}{\partial y^n} \right|_{y=0} = 0 \quad (25)$$

$$\lim_{y \rightarrow \infty} \phi \rightarrow \phi_L. \quad (26)$$

In the above,  $n$  is odd. These conditions impose boundary conditions on  $\delta\phi$ , because  $\phi_L$  is known, and  $\phi = \phi_L + \delta\phi$ .

The distortion field  $\delta\phi(x, y)$  will be found based on an ansatz. Let us evaluate the  $y$ -derivative of the bulk tilted lamellar phase

$$\left. \frac{\partial \phi_L}{\partial y} \right|_{y=0} = -q_y \phi_q \sin(q_x x). \quad (27)$$

Because the distortion of the omegas is well localized near the grain boundary at  $y=0$ , it is therefore reasonable to assume that  $\phi$  has the following form:

$$\phi_\Omega(x, y) = \phi_L(x, y) + f(y) \sin(q_x x). \quad (28)$$

The procedure we adopt is as follows. This ansatz for  $\phi$  is inserted into the free energy density and the integration over  $x$  and  $z$  is carried out. The grain-boundary energy functional  $\gamma$  then depends on the unknown amplitude  $f(y)$ . This is minimized by an Euler-Lagrange equation, which results in a fourth order ordinary differential equation for  $f(y)$ . The boundary conditions, Eqs. (25)–(26), will translate into boundary conditions on  $f(y)$ . The solution of the Euler-Lagrange equation gives, in principle, everything we want to know about the system: spatial distribution of the order parameter, line tension, etc.

We begin by putting our ansatz (28) into the expression (24) for  $\gamma$ . Integration over  $x$  and  $z$  and a little simplification yields

$$\begin{aligned} \gamma[f] = & 2 \int_0^\infty \left\{ \frac{1}{4} q_y^2 \phi_q f \sin q_y y + \frac{1}{4} \left[ 1 - \chi + \phi_0^2 + \frac{1}{4} \phi_q^2 \right. \right. \\ & \times (1 + 2 \sin^2 q_y y) + q_x^4 - q_x^2 \left. \right] f^2 + \frac{1}{2} \phi_q q_y f' \\ & \times \cos q_y y - \frac{1}{4} f'^2 + \frac{1}{2} q^2 \phi_q f'' \sin q_y y - \frac{1}{2} q_x^2 f f'' \\ & \left. + \frac{1}{4} (f'')^2 \right\} dy. \end{aligned} \quad (29)$$

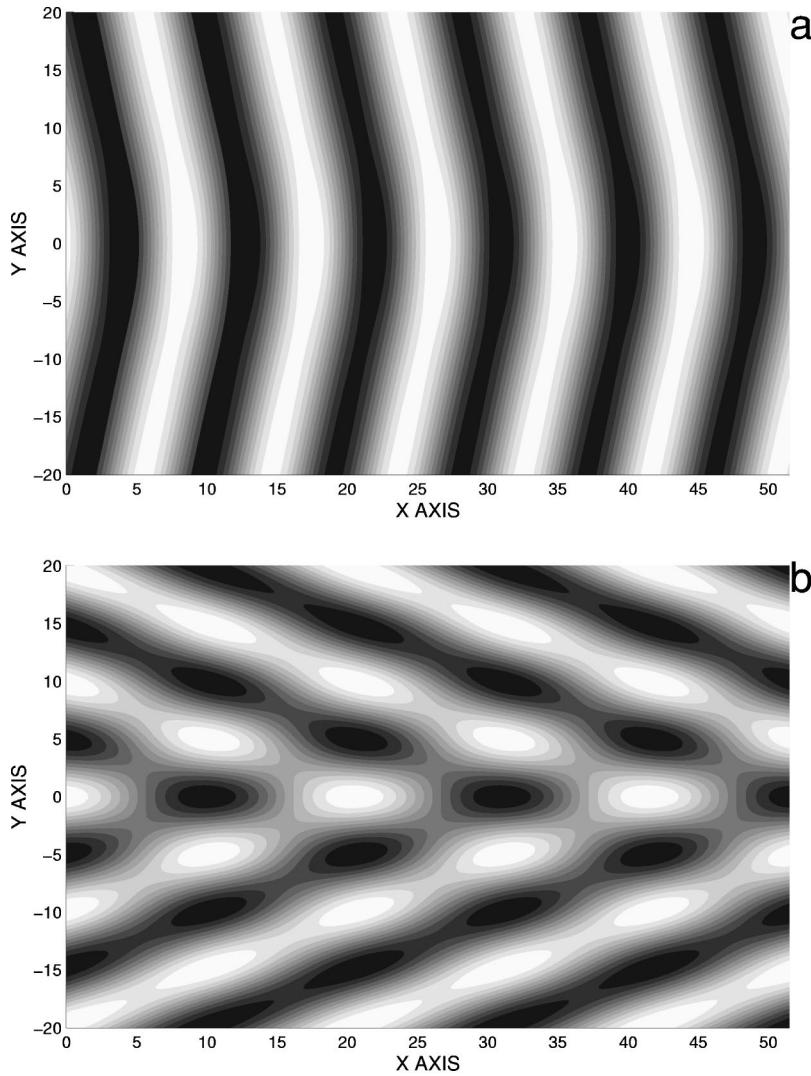


FIG. 3. Same as Fig. 2, but with  $\chi=0.76$ . Top plot is for  $\theta=20^\circ$  and the bottom plot is for  $\theta=130^\circ$ . The system is closer to the ODT than that of Fig. 2, and the modulations of the lamellar thickness are more prominent.

The Euler-Lagrange equation for the function  $f(y)$  is obtained by minimizing Eq. (29)

$$[A + C \cos(2q_y y)]f + Bf'' + f'''' = 0, \quad (30)$$

where  $A$ ,  $B$ , and  $C$  depend on the parameters of the problem as follows:

$$A(\theta) = 1 - \chi + \phi_0^2 + \frac{1}{2} \phi_q^2 + q_x^4 - q_x^2$$

$$B(\theta) = 2q_y^2$$

$$C = -\frac{1}{4} \phi_q^2.$$

Note that the profile Eq. (30) is linear in  $f$  because the free energy, Eq. (24) is second order in  $\delta\phi$ . Equation (30) is similar to the Mathieu equation, which is the Schrödinger equation for an electron in a periodic (sinusoidal) one-dimensional potential as appears in many solid-state physics problems. The parameter  $A$  plays the role of the electron total energy, and  $C$  is the amplitude of the periodic potential. Unlike the solid-state case, here the “energy” parameter  $A$ , the “kinetic term” parameter  $B$  as well as the periodicity of the

“potential” term depend on the angle  $\theta$ , leading to a more complex band structure as function of  $\theta$ . Lastly, the differential equation is of fourth, not second order. Another useful observation is that Eq. (30) is invariant with respect to the spatial variable transformation  $y \rightarrow -y$ . Therefore, the solutions can be classified as symmetric and asymmetric. As we will see, the symmetric and asymmetric solutions do not satisfy separately the boundary conditions, so a combination of them will be needed.

Since this equation is linear with periodic coefficients, a solution to it will have the Bloch form. This is also known as the Floquet theorem [20]

$$f(y) = e^{ky} g(y), \quad (31)$$

where  $g(y)$  is a periodic function with period  $d_y = \pi/q_y$ , which is the same periodicity as appears in Eq. (30). Hence, it is appropriate to write it as a Fourier series

$$g(y) = \sum_{n=-\infty}^{\infty} a_n e^{2inq_y y}. \quad (32)$$

Substituting the Bloch form Eq. (31) into Eq. (30), we get a

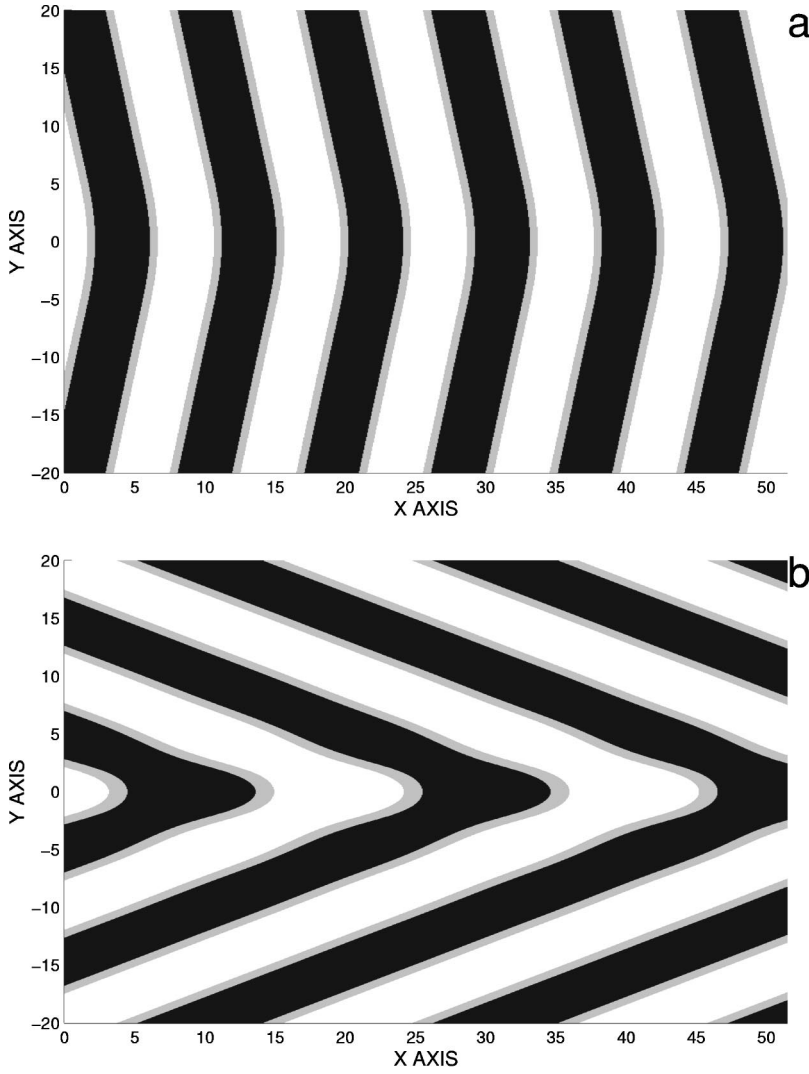


FIG. 4. Black, white and gray contour plot, showing  $A$ -rich,  $B$ -rich, and interfacial regions, respectively. Black regions are  $A$  rich ( $\phi_\Omega > 0.2$ ), white regions are  $B$  rich ( $\phi_\Omega < -0.2$ ), while gray regions marks the interfacial region ( $-0.2 \leq \phi_\Omega \leq 0.2$ ). Top plot is for  $\theta = 20^\circ$  and in the bottom plot  $\theta = 130^\circ$ . The interaction is set to  $\chi = 1$ .

sum of exponential terms. Demanding that the coefficients in front of every exponent vanish, we obtain the following recursion relation:

$$\begin{aligned} & [A + B(k + 2inq_y)^2 + (k + 2inq_y)^4]a_n \\ & + \frac{1}{2}C(a_{n-1} + a_{n+1}) = 0. \end{aligned} \quad (33)$$

The appearance of  $a_{n-1}$  and  $a_{n+1}$  is due to the  $\cos(2q_y y)$  term in Eq. (30). At first glance, it seems that for every  $k$ , choosing “initial values” for the coefficients  $\{a_n\}$  gives a valid solution. However, a closer inspection shows that for an arbitrary  $k$  vector the series  $a_n$  will diverge. Only a very specific value of  $k$  (eigenvalue) will give a convergent series.

The method by which we find this value is as follows (e.g., see Ref. [20]). Rewrite the recursion relations (33) as

$$\frac{a_n}{a_{n-1}} = \frac{-C/2}{A + B(k + 2inq_y)^2 + (k + 2inq_y)^4 + Ca_{n+1}/2a_n}, \quad (34)$$

for  $n > 0$ , and similarly

$$\frac{a_n}{a_{n+1}} = \frac{-C/2}{A + B(k + 2inq_y)^2 + (k + 2inq_y)^4 + Ca_{n-1}/2a_n} \quad (35)$$

for  $n < 0$ . For very large values of  $n$ ,  $a_{n+1}/a_n$  should be much smaller than one, so one can start from some  $N \gg 1$ , assuming that  $a_{N+1}/a_N \rightarrow 0$ , and get

$$\frac{a_N}{a_{N-1}} \approx \frac{-C/2}{A + B(k + 2iNq_y)^2 + (k + 2iNq_y)^4} \quad (36)$$

then iterating *backward* gives the ratios  $\{a_n/a_{n-1}\}$  for  $0 < n \leq N$ . Carrying out the same procedure for negative  $n$ 's one arrives at the *stopping condition*:

$$A + Bk^2 + k^4 = -\frac{1}{2}C \left( \frac{a_{-1}}{a_0} + \frac{a_1}{a_0} \right), \quad (37)$$

from which  $k$  is deduced, because the ratios  $a_1/a_0$  and  $a_{-1}/a_0$  are already known from Eqs. (34)–(35). The iteration scheme is to choose an initial guess for  $k$ , put it in Eq. (36), and use Eqs. (34) and (35) successively for all  $n \neq 0$ . When  $n = 0$  is reached,  $k$  is calculated from Eq. (37), and put back in Eq. (36). The process repeats until convergence is achieved. From the required boundary conditions at infinity,

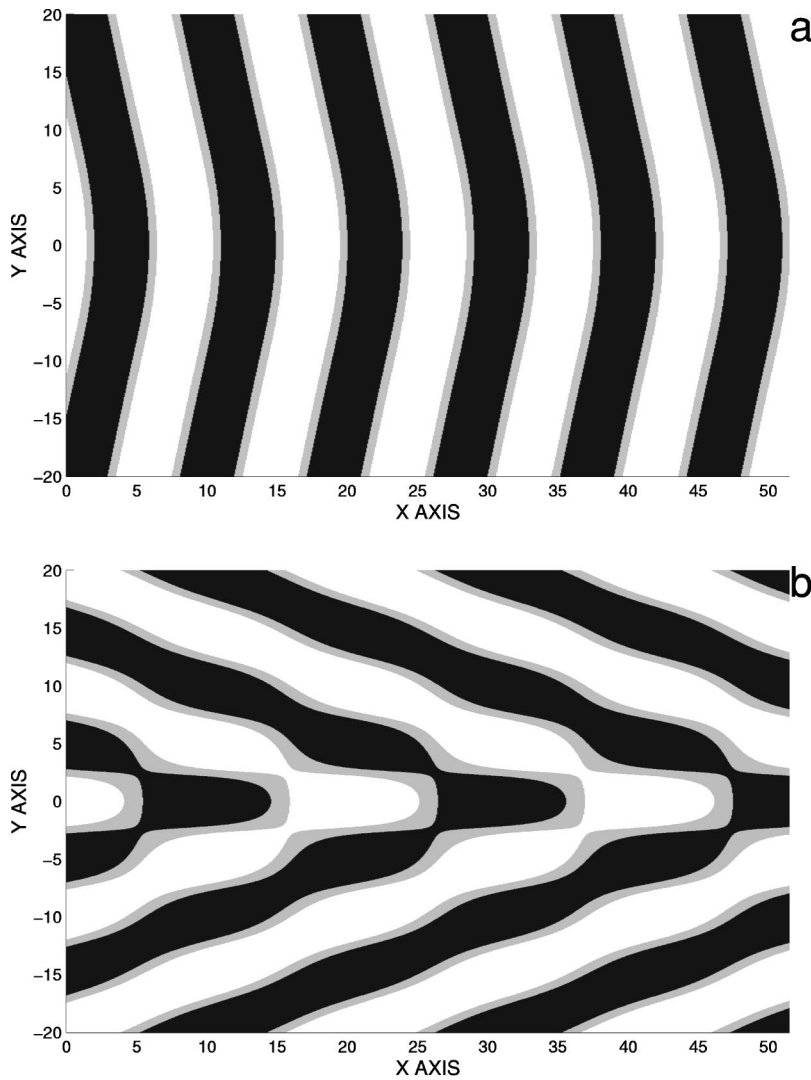


FIG. 5. As in Fig. 4, but with  $\chi=0.76$ . Top plot is for  $\theta=20^\circ$  and the bottom plot is for  $\theta=130^\circ$ . Comparison with Fig. 4 shows that for fixed tilt angle  $\theta$ , the omega structure and the modulations of the lamellar thickness are more evident closer to the ODT.

only  $k$ 's such that  $\text{Re}(k)<0$  are acceptable, recalling that the Bloch form (31) contains an  $e^{ky}$  term.

It can be seen from Eqs. (34) and (35) that if a certain value of  $k$  gives a physical converging solution for  $y \rightarrow \infty$ , then  $k^*$ , the complex conjugate of  $k$ , will also be a convergent solution, but with amplitudes  $a_{-n}^*$ . Solutions with  $-k$  and  $-k^*$  are possible, too, but are discarded because for them  $f(y)$  diverges as  $y \rightarrow \infty$ . The functions with definite symmetry include both  $k$  and  $-k$  and hence diverge at infinity. Consequently, by dropping the  $-k$  solution we choose a specific combination of the symmetric and asymmetric functions with respect to  $y$ . The function  $f$  is a combination of the two independent solutions, and since it is real, it must be equal to

$$f(y) = e^{ky} \sum_{n=-\infty}^{\infty} a_n e^{2inq_y y} + \text{c.c.}, \quad y \geq 0. \quad (38)$$

A choice of  $k$  such that  $\text{Re}(k)<0$  ensures that the disturbance will decay away far enough from the interface,  $y \rightarrow \infty$ . The use of a linearization scheme leaves us with a linear ordinary differential equation, so that we lose the abil-

ity to impose all boundary conditions, and forces us to use only the first and third derivatives of  $f$ , which by the use of Eqs. (7), (25), and (28) are

$$\left. \frac{\partial f}{\partial y} \right|_0 = q_y \phi_q \quad (39)$$

$$\left. \frac{\partial^3 f}{\partial y^3} \right|_0 = -q_y^3 \phi_q. \quad (40)$$

In summary, the series  $\{a_n\}$  can be determined from the recursion relations (35) and (34), while the only remaining unknown is the complex parameter  $a_0$ . The function  $f(y)$  itself depends on this series as well as on the two boundary conditions. Substitution of Eq. (38) in the above boundary conditions fully determines both the phase and magnitude of  $a_0$  and therefore sets the complete solution to the problem.

### Band gaps and degeneracy

In the usual Schrödinger equation for periodic potentials, one encounter energetic gaps in the energy spectrum. They occur whenever the  $k$  vector crosses the edges of a Brillouin

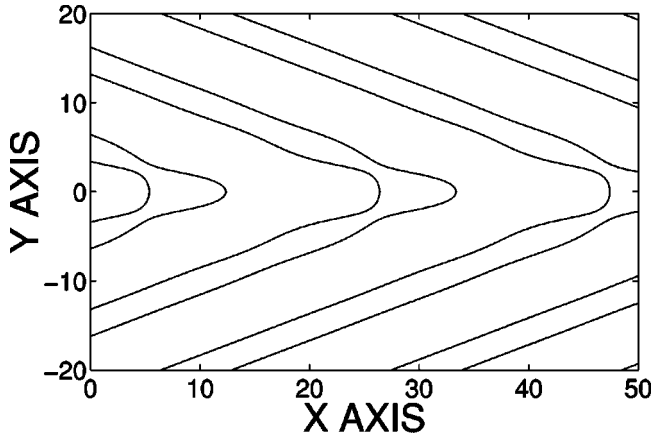


FIG. 6. Plot of the equi- $\phi$  contour lines corresponding to  $\phi=0.5$ , with the same conditions as in Fig. 4(b). Although the profile shown in Fig. 4 is symmetric with respect to the interchange of  $A$  and  $B$ , clearly the leading and trailing edges of the lamellae are not identical.

zone. It should be expected that similar phenomenon happens here, too. Indeed, in our case it will happen whenever

$$\text{Im}(k) = m q_y, \quad (41)$$

for some integer  $m$ . For  $k$  fulfilling (41) there is a *degeneracy* in the two previously found solutions. It can be seen by noticing that if Eq. (41) holds,  $k$  and  $k^*$  differ by  $2imq_y$ . Therefore, the amplitudes  $\{a_n\}$  corresponding to the eigenvalue  $k^*$  are the same as those  $\{a_{n-1}\}$  corresponding to  $k$ , and the two solutions are dependent. If  $m$  is even, the two solutions are real. One can see this by using  $k = k_r + 2inq_y$  ( $n$  being an integer) and noticing that

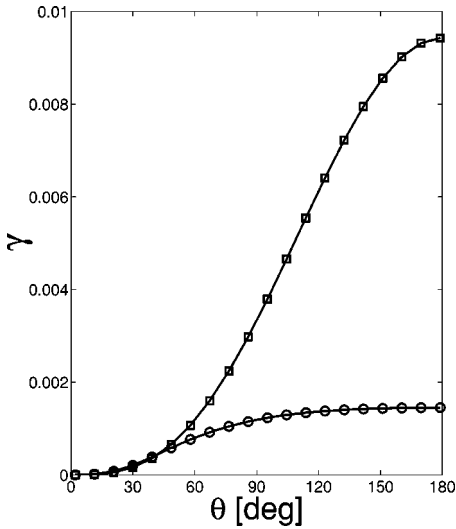


FIG. 7. Plot of the grain-boundary energy  $\gamma$  as function of the tilt angle  $\theta$ , for  $\chi=0.76$ .  $\theta$  ranges from 0 to 180°. The curve marked with rectangles shows the results obtained in Sec. III for the chevron morphology, with  $\gamma = \frac{2}{3} \phi_q^2 q_y^3$ . The curve with circles shows the results of Sec. IV. Notice that the two expressions are very similar, but at some intermediate values of  $\theta$  ( $\theta \approx 50^\circ$ ) there is a crossover from the chevron to the omega morphology. Evidently, for large tilt angles the omegas cost less energy than the chevron.

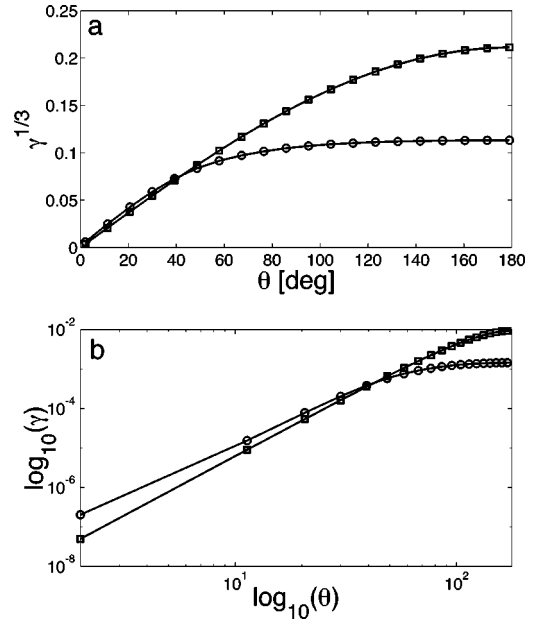


FIG. 8. In (a) the grain-boundary energy  $\gamma$  of Fig. 7, is plotted as  $\gamma^{1/3}$  against the tilt angle  $\theta$ . The curve marked with rectangles is straight for small angles, depicting perfect  $\gamma \sim \theta^3$  dependence. The curve marked with circles shows a power exponent 2.91. In (b) the two line tension are plotted on a log-log plot. The results of Sec. III show  $\theta^3$  scaling, while the omegas show a smaller power exponent. Possible small numerical errors in our scheme to find the wavevector  $k$  are important for small angles (the leftmost point being at  $\theta=2^\circ$ ), and this may easily change the line tension exponent from the expected 3 to 2.91.

$$e^{(k_r + 2inq_y)y} \sum_{n=-\infty}^{\infty} a_n e^{2inq_y y} = e^{k_r y} \sum_{n=-\infty}^{\infty} a_{n-1} e^{2inq_y y}. \quad (42)$$

Using the right term of Eq. (42) in the iteration process, we see that  $a_n = (a_{-n})^*$ , and  $f(y)$  is real.

In these band gaps there is a *splitting* of the real part of  $k$ ; another *independent*  $k$  vector appears whose imaginary part is the same, but which has a different real part. This is clearly seen in Fig. 8(a), where the band gaps appear to be centered around 18°, 26°, and 42°. The last gap occurs for  $\theta > 127^\circ$ .

The two solutions constructed by the Bloch form (31) are obviously independent. It should be noted that the appearance of energy gaps is a mathematical consequence which does not introduce any singularity into the physical grain-boundary energy. It is due to our approximative linearization scheme, and is not expected to occur if nonlinearity would have been included.

## V. CHEVRONS AND OMEGA-LIKE PROFILES

We discuss the results obtained by using the analytical eigenvalue scheme detailed above. For small angles (small tilt) the response of the system is weak. Namely, the lamellae gradually change their orientation and the profile is well described by the analytical chevron form, Eq. (20). At higher tilt angles the polymer chains at the interface are stretched much more than their preferred length. Here, our analytical scheme (Sec. IV) gives rise to profile shape quite different

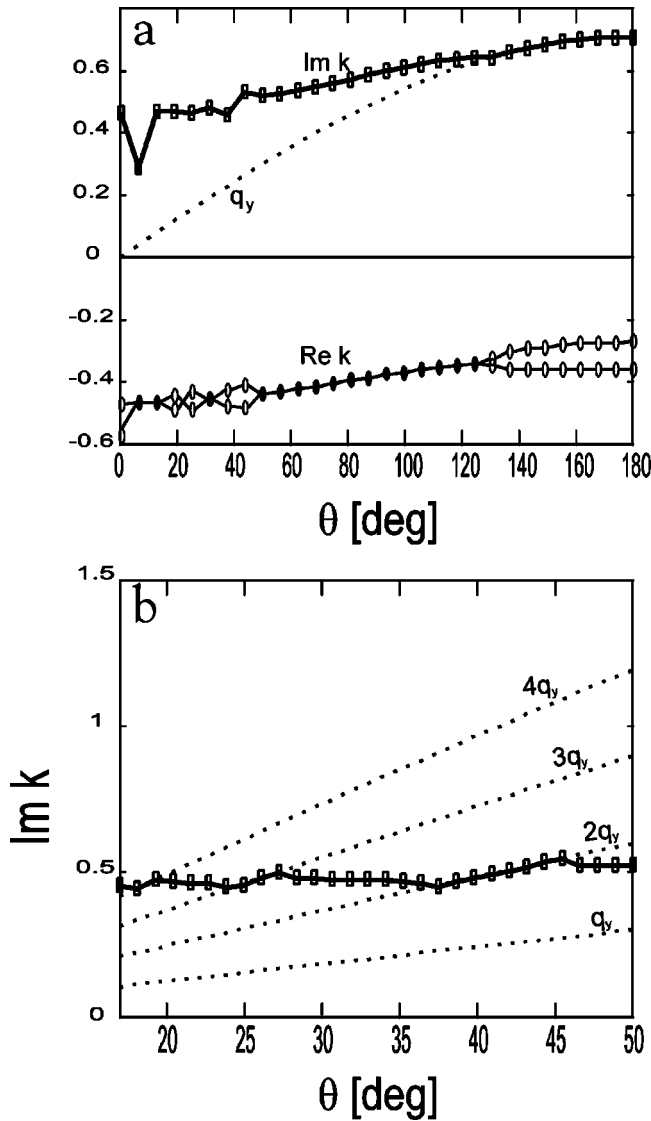


FIG. 9. The imaginary and real parts of the wave vector  $k$  in expression (31) are shown in (a), for  $\chi=1$ . The line with rectangles corresponds to the imaginary part. Only the positive imaginary part is shown. The line with circles corresponds to the real part of  $k$ . Dotted line shows  $q_y$ , being the characteristic length scale in the  $y$  direction. Notice the splitting of the real part of  $k$  in the band gaps. An enlargement of the same curve of the imaginary part of  $k$ , for  $17^\circ \leq \theta \leq 50^\circ$  is shown in (b). The black lines indicates integer multiples of  $q_y$  in order to show the regions of degeneracy. Three band gaps are shown, around  $18^\circ$ ,  $26^\circ$ , and  $42^\circ$ . In these gaps  $\text{Im}(k) = imq_y$  for some integer  $m$ .

than those obtained in Sec. III for the chevron.

Figure 2 shows contour plots of the order parameter profile  $\phi_\Omega(x,y)$ . We have taken the average of the order parameter,  $\phi_0$ , to be zero. The gray levels indicate the magnitude of the order parameter: black regions corresponding to the maximum values of  $\phi_\Omega$  (rich in  $A$  polymer), while white to its minimum value (rich in  $B$  polymer). The interaction is set to  $\chi=1$ . In Fig. 2(a), the chevron morphology is represented using the results of Sec. IV, with tilt angle  $\theta=20^\circ$ . The plot is identical when using the expressions of Sec. III. A smooth changeover between the two lamellar phases is observed. The chevron solution follows nicely the analytical form of

Eq. (20). For large angles ( $\theta=130^\circ$ ), the omega structure takes over as is shown in Fig. 2(b), with large protrusions of the lamellae at the interface. As is explained below, for large angles the excessive packing frustration of the chevrons cost more energy than the  $\Omega$ . Chevron and  $\Omega$  morphologies are also shown in Fig. 3 but with  $\chi=0.76$  much closer to its critical value of  $\frac{3}{4}$ . As one goes away from the  $y=0$  interface, undulations of  $\phi_\Omega$  are encountered. There are more of them as the order-to-disorder transition (ODT) is approached, and the omega structure is more evident.

Figures 4 and 5 show the same plots, but with the lines of interface enhanced. The regions in white, gray, and black correspond to  $\phi_\Omega < -0.2$ ,  $-0.2 \leq \phi_\Omega \leq 0.2$ , and  $\phi_\Omega > 0.2$ , respectively. The gray marks the interface between the  $A$  and  $B$  rich regions. The equi- $\phi_\Omega$  lines clearly show the form of the interface in the chevron and omega morphologies. Notice that as the ODT is approached ( $\chi=0.76$  in Fig. 5), there are more undulations apparent on top of the bulk lamellar phase. In the chevron regime, the  $A/B$  interfacial width remains almost uniform, while in the omega regime it varies close to the kink [8]. Figure 4 shows quite clearly that the leading and trailing edges of the lamellae are quite different when the angle of the grain boundary is large. This is emphasized in Fig. 6, for  $\theta=130^\circ$  and  $\chi=1.0$ , the same conditions of the lower plot of Fig. 4. The lines indicate where  $\phi=0.5$ . That the protrusion at the leading edge is much more pronounced than at the trailing edge is quite reminiscent of the profiles seen in experiment [3] with one exception; in experiment, only half of the lamellae look this way, the other half hardly display protrusions at all; that is, the symmetry between positive and negative order parameter domains is broken.

Results for the grain-boundary energy  $\gamma_{TB}$  are shown in Fig. 7. The  $\chi$  parameter is arbitrarily fixed to be  $\chi=0.76$ . We show the grain-boundary energy calculated analytically by means of the methods of Sec. III and which is valid for small  $\theta$ , as well as that calculated in Sec. IV. The grain-boundary energy  $\gamma_{TB}$  is an increasing function of the angle  $\theta$ . In the small angle regime the grain-boundary energy obtained in Sec. III scales as  $\gamma \sim \theta^3$ . This scaling is also satisfied (to a good approximation) by the solutions obtained in Sec. IV. To see this, the same data is plotted in a different fashion in Fig. 8. In Fig. 8(a)  $\gamma^{1/3}$  is plotted as function of  $\theta$ , while in Fig. 8(b) the data is plotted on a log-log plot. From both parts of Fig. 8 we conclude that the solution obtained in Sec. IV gives a power law with exponent of 2.91. Accuracy of the leftmost point of the solid curve in Fig. 8(b) is doubtful, due to poor convergence of the numerical iteration scheme for small angles,  $\theta < 5^\circ$ . As the tilt angle grows, deviations from the  $\theta^3$  behavior become larger, and the omega morphology, with its lower energy, appears gradually.

For intermediate and large angles, our results are supported by a full numerical solution of this problem [2]. Presumably, for small angles there is agreement too. This needs to be further checked since in Ref. [2] the smallest angle was  $\theta=28^\circ$ . Note that in contrast to the full numerical solution in which the order parameter profile was obtained via a functional minimization, here we employed numerical means only to obtain the value of the eigenvalue  $k$ , while the profile equation was solved analytically.

In Fig. 9 we show the  $k$  vectors found by the use of the iteration scheme, as a function of tilt angle  $\theta$ , with  $\chi=1$

fixed. Outside of the band-gaps,  $k$  and  $k^*$  are valid solutions, so for clarity only the  $k$  with  $\text{Im}(k) > 0$  is shown. Notice that  $\text{Re}(k)$  is always negative. The band gaps are clearly seen on this graph as regions where  $\text{Re}(k)$  have two distinct values (hollow circles). A check on the imaginary part of  $k$  in these regions reveals that it is an integer multiple of  $q_y$ .

Our results agree well with experiment with the exception that we do not obtain the symmetry-breaking transition of the omega morphology [8]. To do so, one must add to an ansatz for the order parameter at least a term which varies as  $2q_x x$ , in addition to the fundamental term varying as  $q_x x$ .

## VI. CONCLUDING REMARKS

We have used a simple Ginzburg-Landau free energy functional to investigate the profiles between lamellar phases of diblock copolymer. Our analytic results give good qualitative agreement with experiment in the weak segregation regime, and with full numerical solution of the same free energy model. The observed chevron morphology develops gradually into an omega morphology for intermediate tilt angles. For small angles, the use of a periodic order parameter with constant amplitude but varying wavevector suffices to describe the order parameter profile. This is well described by the chevron morphology. For intermediate angles the change of the profile at the interface deviates significantly from the bulk, and requires a different treatment. The devia-

tion from the bulk lamellae was found, and gave rise to the protrusion characterizing the omega morphology. The symmetry breaking of this phase was not obtained.

We were able to calculate grain-boundary energies and to determine that they scale as the cube of the angle [2,18] for small angles. As the tilt angle grows into the intermediate regime, the profiles deviate continuously from the chevron shape. As the angle approaches  $180^\circ$ , the energy must go to zero because the grain boundary vanishes at that angle. This does not occur in our analytic derivation, since, for such large angles, the linearization assumption is no longer valid.

Interesting extensions of the present paper would describe interfaces of two perpendicular lamellar phases (so-called  $T$  junctions), interfaces between modulated phases of other symmetries, and the inclusion of a twist instead of a tilt [21,22].

## ACKNOWLEDGMENTS

We benefited from discussions with Y. Cohen, S. Gido, R. Netz, P. Rosenau, M. Schwartz, and E. Thomas. Partial support from the U.S.-Israel Binational Foundation (B.S.F.) under Grant No. 98-00429, the National Science Foundation under Grant No. DMR 9876864, and the Israel Science Foundation founded by the Israel Academy of Sciences and Humanities-Centers of Excellence Program is gratefully acknowledged.

- 
- [1] M. Seul and D. Andelman, *Science* **267**, 476 (1995).  
 [2] R. R. Netz, D. Andelman, and M. Schick, *Phys. Rev. Lett.* **79**, 1058 (1997).  
 [3] S. P. Gido and E. L. Thomas, *Macromolecules* **27**, 6137 (1994).  
 [4] Y. Nishikawa, H. Kawada, H. Hasegawa, and T. Hashimoto, *Acta Polym.* **44**, 192 (1993); T. Hashimoto, S. Koizumi, and H. Hasegawa, *Macromolecules* **27**, 1562 (1994).  
 [5] L. Leibler, *Macromolecules* **13**, 1602 (1980).  
 [6] G. H. Fredrickson and E. Helfand, *J. Chem. Phys.* **87**, 697 (1987).  
 [7] M. W. Matsen and F. Bates, *Macromolecules* **29**, 7641 (1996).  
 [8] M. W. Matsen, *J. Chem. Phys.* **107**, 8110 (1997).  
 [9] S. Villain-Guillot, R. R. Netz, D. Andelman, and M. Schick, *Physica A* **249**, 285 (1998); S. Villain-Guillot and D. Andelman, *Eur. Phys. J. B* **4**, 95 (1998).  
 [10] G. Gompper and M. Schick, *Phys. Rev. Lett.* **65**, 1116 (1990).  
 [11] D. Andelman, F. Brochard, and J.-F. Joanny, *J. Chem. Phys.* **86**, 3673 (1987).  
 [12] T. Garel and S. Doniach, *Phys. Rev. B* **26**, 325 (1982).  
 [13] P. J. Flory, *Principles of Polymer Chemistry* (Cornell University, Ithaca, 1953).  
 [14] Note that when  $\chi_f$  takes the value  $\chi_f^*$  so that  $c_1 = 0$ , one might expect a continuous order-disorder transition in the symmetric  $A/B$  system to a uniform phase, as occurs in ordinary phase separation. However as will be shown, this transition is preempted by a continuous transition to a modulated phase which occurs at  $\chi = \chi_f / \chi_f^* = 3/4$ . At this value,  $c_1$  is still positive.  
 [15] R. J. Spontak, J. C. Fung, M. B. Braunfeld, J. W. Sedat, D. A. Agard, L. Kane, S. D. Smith, M. M. Satkowsky, A. Ashraf, D. A. Hajduk, and S. M. Gruner, *Macromolecules* **29**, 4494 (1996).  
 [16] G. H. Fredrickson and K. Binder, *J. Chem. Phys.* **91**, 7265 (1989).  
 [17] I. W. Hamley and V. E. Podneps, *Macromolecules* **30**, 3701 (1997).  
 [18] P. G. de Gennes and J. Prost, *The Physics of Liquid Crystals*, 2nd ed. (Clarendon, Oxford, 1993), p. 484.  
 [19] A. C. Newell, T. Passot, C. Bowman, N. Ercolani, and R. Indik, *Physica D* **97**, 185 (1996).  
 [20] P. M. Morse and H. Feshbach, *Methods of Theoretical Physics* (McGraw-Hill, New York, 1953), pp. 557 and 558.  
 [21] S. P. Gido, J. Gunther, E. L. Thomas, and D. Hoffman, *Macromolecules* **26**, 4506 (1993); S. P. Gido and E. L. Thomas, *ibid.* **27**, 849 (1994).  
 [22] R. D. Kamien and T. C. Lubensky, *Phys. Rev. Lett.* **82**, 2892 (1999).